

Two-photon fluorescence absorption and emission spectra of dyes relevant for cell imaging

F. BESTVATER*, E. SPIESS*, G. STOBRAWA†, M. HACKER†,
T. FEURER†, T. PORWOL‡, U. BERCHNER-PFANNSCHMIDT‡,
C. WOTZLAW‡ & H. ACKER‡

*Biomedizinische Strukturforchung (A0602), Deutsches Krebsforschungszentrum, PO Box 101949, D-69009 Heidelberg, Germany

†Institut für Optik und Quantenelektronik, Friedrich-Schiller-Universität, D-07743 Jena, Germany

‡Max-Planck-Institut für Molekulare Physiologie, D-44227 Dortmund, Germany

Key words. 3D reconstruction, fluorochromes, live cell imaging, MPM, non-linear microscopy, spectra, TPE, two-photon excitation.

Summary

Two-photon absorption and emission spectra for fluorophores relevant in cell imaging were measured using a 45 fs Ti:sapphire laser, a continuously tuneable optical parametric amplifier for the excitation range 580–1150 nm and an optical multichannel analyser. The measurements included DNA stains, fluorescent dyes coupled to antibodies as well as organelle trackers, e.g. Alexa and Bodipy dyes, Cy2, Cy3, DAPI, Hoechst 33342, propidium iodide, FITC and rhodamine. In accordance with the two-photon excitation theory, the majority of the investigated fluorochromes did not reveal significant discrepancies between the two-photon and the one-photon emission spectra. However, a blue-shift of the absorption maxima ranging from a few nanometres up to considerably differing courses of the spectrum was found for most fluorochromes. The potential of non-linear laser scanning fluorescence microscopy is demonstrated here by visualizing multiple intracellular structures in living cells. Combined with 3D reconstruction techniques, this approach gives a deeper insight into the spatial relationships of subcellular organelles.

Introduction

Non-linear microscopy became available with the invention of two-photon laser scanning microscopes (TPLSM) (Sheppard, 1977; Denk *et al.*, 1990). With the introduction of reliable turn-key femtosecond oscillators (Denk *et al.*, 1995; Denk & Svoboda, 1997), multiphoton microscopy (MPM) in general developed into a versatile tool in many fields of biomedical research (Piston, 1999; Brown *et al.*, 2001; Gratton *et al.*, 2001; Williams *et al.*, 2001).

Many reasons favour the use of MPM. Digital wide-field microscopy is limited in sensitivity and spatial resolution because of out-of-focus background fluorescence and, to a lesser extent, this also applies to conventional one-photon confocal laser scanning microscopy. Against it, in MPM the high photon density required for the very low probability of near-simultaneous absorption of two photons and thus generation of fluorescence is only achieved at the beam focus. Limiting the illumination of a sample to a femtolitre volume, MPM is used especially for the investigation of living systems in both biology and medicine. The great advantages of MPM include extended sample penetration and lower impact on specimen and fluorochrome. A closer insight into technical details, discussion of advantages and applications may be obtained elsewhere (Williams *et al.*, 1994, 2001; Denk *et al.*, 1995; Centonze & White, 1998; Periasamy *et al.*, 1999; Piston, 1999; König, 2000; Patterson & Piston, 2000). Although biomedical applications of MPM are steadily increasing, the technique still suffers from the need for universal fluorescence staining methods of living cells and tissues, as well as from insufficient knowledge regarding the absorption and emission spectra or cross-sections of relevant fluorochromes. The latter point is essential for proper applications and optimal results. Lack of spectra was considered unfortunate from the beginning (Smith, 1986; Williams *et al.*, 1994; Xu & Webb, 1996) and, to date, publications related to this subject are rare and cover only a limited range of fluorochromes (Birge, 1986; Xu & Webb, 1996; Xu *et al.*, 1996; Malak *et al.*, 1997; Albota *et al.*, 1998; Fisher *et al.*, 1998; Gratton *et al.*, 2001). It is difficult to estimate multiphoton absorption spectra from one-photon data because of different selection rules and the distinct effects of vibronic coupling (Xu *et al.*, 1996). Although, in theory, similar emission characteristics for both one-photon excitation (OPE) and two-photon excitation (TPE) are predicted, in practice a blue shift of TPE vs. OPE spectra was observed (Albota *et al.*,

1998). Therefore, making a comparative study seems reasonable; the essential experimental data are presented here.

In contrast to OPE, in TPE tuning the laser power constitutes an additional control parameter, which may be used to efficiently excite different local maxima. Therefore, it is important to know the exact profile of the absorption spectra of the fluorochromes for optimal excitation of individual fluorophores in a multiply stained specimen. In this study we aim to analyse absorption and emission data of fluorochromes frequently used in cell biology and physiology.

In order to extend TPE applications beyond one fluorochrome it has become common practice to tune the Ti:sapphire laser excitation wavelength for optimal power exploitation as well as for fluorescence excitation of many common fluorochromes used in multichannel applications (Xu *et al.*, 1996; Straub *et al.*, 2000). In this study we present a further example of this approach by recording images of the same specimen at 860 nm excitation in four different channels. Nevertheless, it

should be emphasized that the experimental determination of the two-photon absorption spectra is a crucial ingredient for microscopy, and future efforts in TPLSM development should be aimed at ensuring optimal excitation for each fluorochrome.

Materials and methods

Fluorochromes

The fluorochromes used are summarized in Table 1. For the measurements, they were dissolved in phosphate buffered saline (PBS) or dimethyl sulfoxide (DMSO). Possible autofluorescence of the solvents was excluded by control measurements. Fusion genes encoding cellular proteins and green fluorescent protein variants (GFPs) were constructed and expressed in human cells as described previously (Bestvater *et al.*, 2002).

Table 1. Spectral characteristics of the investigated fluorochromes.

Fluorochrome	Absorption (nm)	Emission ^a (nm)	Source ^b	Specificity/application
Acridine Orange	— ^c	— ^c	Se (10665)	Nucleic acids
Alexa Fluor 488	491	515 ¹	MP (A-11001)	AB label
Alexa Fluor 546	553	569 ¹	MP (A-11003)	AB label
Alexa Fluor 594	594	610 ¹	MP (A-10239)	AB label
aminomethylcoumarin (AMC) methylcoumarin	346	443 ³	Ba (I-1050)	Leaving group/AB label
	359	447 ³		
Bodipy FL ^d	505	511 ¹	MP (D-3521)	Diverse, e.g. AB label
Bodipy TRoad	589	617 ¹	MP (D-7540)	Diverse, e.g. AB label
Cy2-IgG	489	506 ¹	Ro	AB label
Cy3-IgG	558	583 ¹	Di	AB label
DAPI	358	461 ²	Si (D-9542)	Nucleic acids
ER-Tracker blue/white	374	575 ¹	MP (E-12353)	Endoplasmic reticulum
F-DTAF-IgG	492	520 ¹	Di	AB label
FITC-IgG	490/495	525/519 ²	Di	AB label
H ₂ DCFDA ^d	500	530 ¹	MP (D-399)	Diverse, e.g. cell organelle staining
Hoechst 33342	352	461 ²	Fl	Nucleic acids
Lissamine rhodamine-IgG	575/570	595/590 ²	Di	AB label
LysoTracker Red	577	590 ¹	MP (L-7528)	Lysosomes, acidic comp.
LysoTracker Yellow	534	551 ¹	MP (L-7527)	Lysosomes, acidic comp.
MitoTracker Red CMX	579	599 ¹	MP (M-7513)	Mitochondria
Phen-Green FL	492	517 ¹	MP (P-6763)	Heavy metal indicator
propidium iodide	536	617 ²	Si (P-4170)	Nucleic acids
quinacrine	423	503 ²	Si (Q-3251)	Nucleic acids, acidic compartments
RedX-IgG	575	600 ¹	Di	AB label
rhodamine 123	507	529–534 ¹	MP (R-302)	Diverse, e.g. AB label
SNARF-1	515/575	575/650 ¹	MP (S-3057)	Physiological pH indicator
Texas Red-IgG	596/589	615/615 ¹	Di	AB label
Texas Red-Phalloidin	577	620 ¹	MP (T-7471)	AB label

^aData from: ¹supplier; ²*Current Protocols in Cell Biology*; ³<http://facs.scripps.edu/spectra>

^bBa: Bachem, Heidelberg, Germany; Di: Dianova, Hamburg, Germany; Fl: Fluka, Buchs, Switzerland; MP: Molecular Probes, Eugene, OR, USA; Ro: Rockland, Gilbertville, USA; Se: Serva, Heidelberg, Germany; Si: Sigma, Deisenhofen, Germany.

^cPure Acridine Orange has broad excitation and emission spectra.

^dDissolved in DMSO.

Spectra acquisition

The experimental set-up to measure the spectra is shown in Fig. 1. It consists of three units. Firstly, a Ti:sapphire laser delivering 45 fs long pulses at 804 nm with a pulse energy of 1 mJ and a repetition rate of 1 kHz. The spectrum and the pulse width were constantly monitored using a spectrometer and a second-order intensity autocorrelator. Secondly, an optical parametric amplifier (TOPAS), which was continuously tunable in the wavelength range between 580 nm and 1150 nm. Figure 2 shows the energy per pulse as a function of the wavelength for the two wavelength ranges used. The output of the parametric amplifier was focused through a 2-mm thick fused silica cuvette using a fused silica lens with a focal length of 400 mm. The distance between the cuvette and the lens was

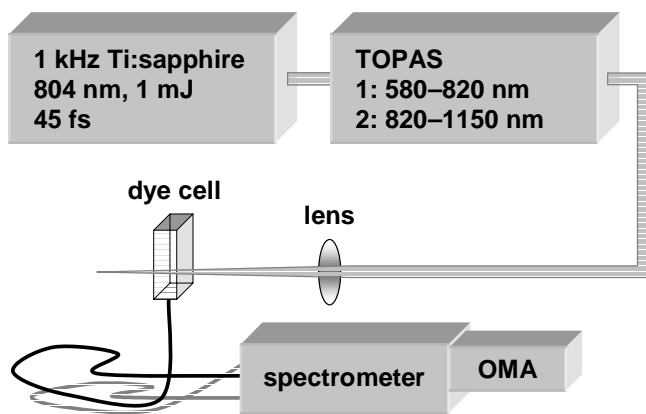


Fig. 1. Experimental set-up for TPE spectra acquisition: The modulated laser pulses (TOPAS) were focused into a dye cell and the excited fluorescence was collected by a multimode fibre. The fibre was connected to a grating spectrometer equipped with an optical multichannel analyser (OMA).

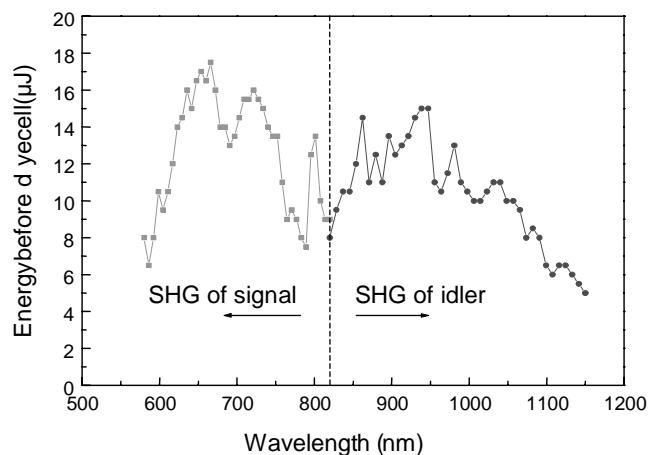


Fig. 2. Pulse energy as a function of wavelength for both scan ranges. (SHG: second harmonic generation).

adjusted such that no white light generation was observed throughout the whole range of excitation wavelengths. The intensity at the sample was estimated as 100 GW cm^{-2} , which corresponds to $\sim 1.6 \times 10^8$ photons cm^{-3} and is sufficient for TPE. As a result of chromatic errors of the focusing lens, the beam diameter varied by $\pm 5.5\%$ in the spectral range from 600 nm to 1200 nm with respect to the beam diameter measured at 900 nm. The fluorescence was collected perpendicular to the direction of the excitation beam by a multimode optical fibre, which was connected to a grating spectrometer. Thirdly, an optical multichannel analyser with 1024 pixels was used to record simultaneously the emission spectrum in the range 260–720 nm. In order to measure the absorption spectra, the excitation wavelength was changed in equidistant steps and for each step 200 single fluorescence spectra were averaged. To extract the absorption as a function of the excitation wavelength, the fluorescence curve was integrated and the result was divided by the square of the excitation intensity assuming a two-photon absorption process (Fisher *et al.*, 1998).

TPE microscopical set-up

The laser source consisted of a Ti:sapphire laser (Coherent Mira 900-F, Dieburg, Germany) pumped by an Ar^+ ion laser. The output was tuneable between 720 nm and 910 nm, the repetition rate was 76 Hz and the pulse duration was typically 110 fs. The pulses were coupled into a mono-mode optical fibre connected to the scan unit PCM 2000 (Nikon, Düsseldorf, Germany) mounted on a conventional fluorescence microscope (TE 300, Nikon). The dispersion of the optical fibre was pre-compensated by a dispersion compensator consisting of a pair of gratings (GDC). For image acquisition, a 60 \times water objective was used (Plan Apochromat DIC H, NA 1.2; Nikon). The fluorescence was detected by a photo multiplier, digitized, and visualized by the EZ 2000 software (Version 2.1.4, Coord Automatisering, the Netherlands). A piezo stepper motor was used for optical sectioning in 500 μm steps. Different fluorescence channels were recorded consecutively.

Image restoration

The spatial data were reconstructed from image stacks with the Amira™ software (TGS, Düsseldorf, Germany). An appropriate threshold was determined to reveal regions of higher intensity. Areas of equal fluorescence intensity were rendered as isosurfaces and false colour look-up tables (LUTs) were applied to distinguish the fluorochromes from each other.

Results and discussion

Fluorescence spectra

Spectral data were recorded from a selection of fluorochromes frequently used in cell studies for direct organelle staining,

antibody labelling and monitoring of biochemical or physiological processes. The data obtained from the measurements are presented in Figs 3–5; in Table 2 the corresponding absorption and emission maxima are compiled. In most cases, the TPE absorption data differ considerably from the expected values derived from the twofold OPE data and a significant blue shift for the TPE values is observed. The comparison of TPE vs. OPE emission maxima (Table 2) reveals heterogeneous results. In 13 cases there are no significant differences (± 7 nm) and 12 further fluorochromes show only minor deviations (7–15 nm), but in the case of BODIPY TR, a considerable difference was found. Deviations up to 15 nm might result from calibration errors intensified by an existing small difference and thus are not likely to be attributed to TPE-specific effects. Both propidium iodide (PI) and aminomethylcoumarin (AMC) exhibit biphasic TPE emission spectra. Although we cannot suggest any explanation for this behaviour in the case of AMC, it is remarkable that the lower maximum of the PI spectrum corresponds to the OPE optimum, but the main TPE maximum at 657 nm is located within the trailing slope of the OPE spectrum. The OPE local maximum of free PI in the green emission light at 515 nm is not represented in the TPE spectrum. The TPE maximum of BODIPY TR coincides with a local OPE maximum. Altogether, almost all of the emission spectra are red-shifted. A conceivable contribution of the dilution buffer to the spectral characteristics of the fluorochromes could be excluded, as described in the Materials and methods section.

Blue shifts of TPE absorption peaks have been reported previously (Xu *et al.*, 1996; Albota *et al.*, 1998). The authors attribute this to parity selection rules, which favour induction of absorption to higher energy levels in TPE. This leads to coincidence of the local TPE maxima with side peaks of OPE. According to both authors, the blue shift is of benefit in MPM, as it allows the use of widely available near infrared lasers and suggests the application of a single wavelength for excitation of several fluorophores with disparate emission characteristics.

In an earlier study, Xu & Webb (1996) found no differences in the emission spectra generated by OPE or TPE for the four fluorochromes they observed (Fluorescein, DiI, Rhodamin B and Lucifer Yellow). Most of our results confirm this outcome; however, in certain cases we found a considerable red shift and also a tendency for the shifted TPE maxima to coincide with side maxima of the OPE spectra. This underlines the authenticity of our measurements.

Microscopical imaging

In consideration of an optimal power exploitation of commercially available lasers, it has become common practice to use a single excitation wavelength for several fluorochromes. Hell *et al.* (1998) used 647 nm to visualize multiple nuclear stainings. In the present case an excitation with 860 nm was applied for a wide range of fluorochromes: Hoechst 33342,

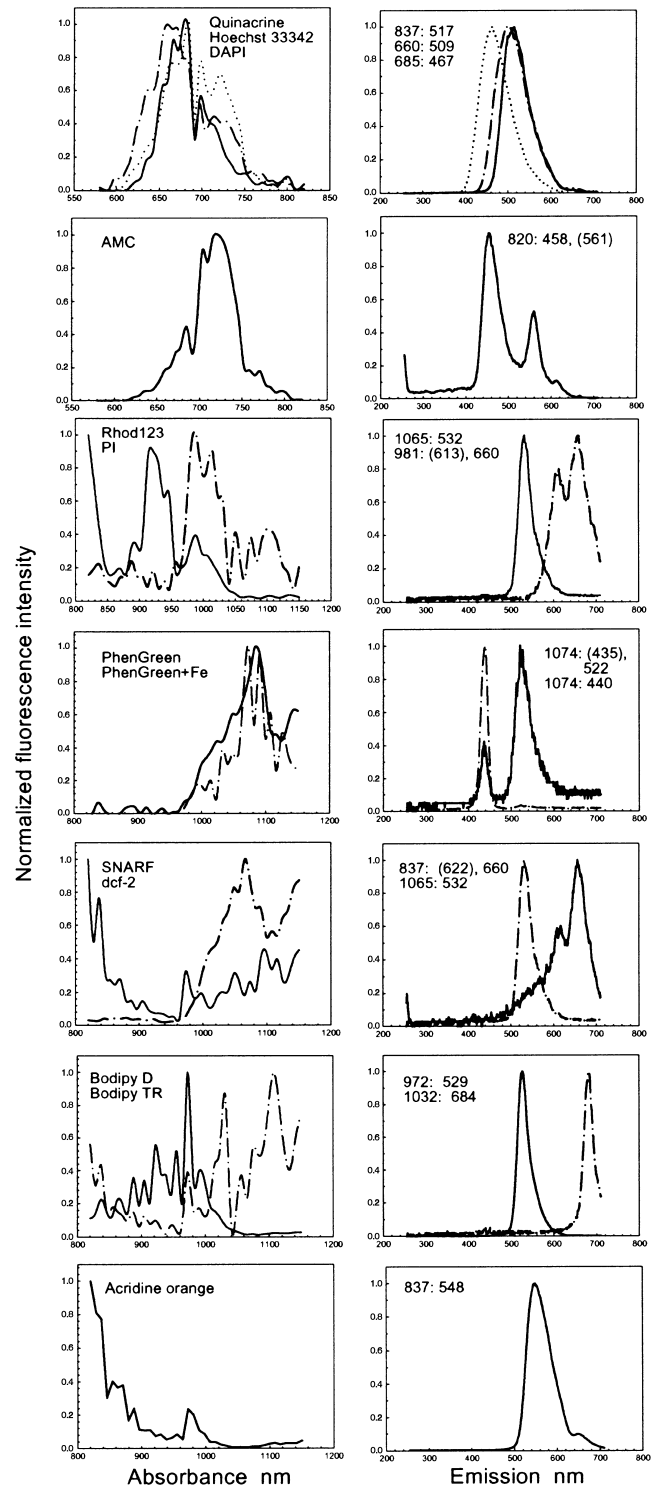


Fig. 3. TPE absorption and emission spectra of fluorochrome dyes. In each plot the first dye is indicated by a solid line, the second by a dash-dotted line and the last by a dotted line, if applicable. For the emission spectra, the applied excitation wavelength and the maximum of emission are specified.

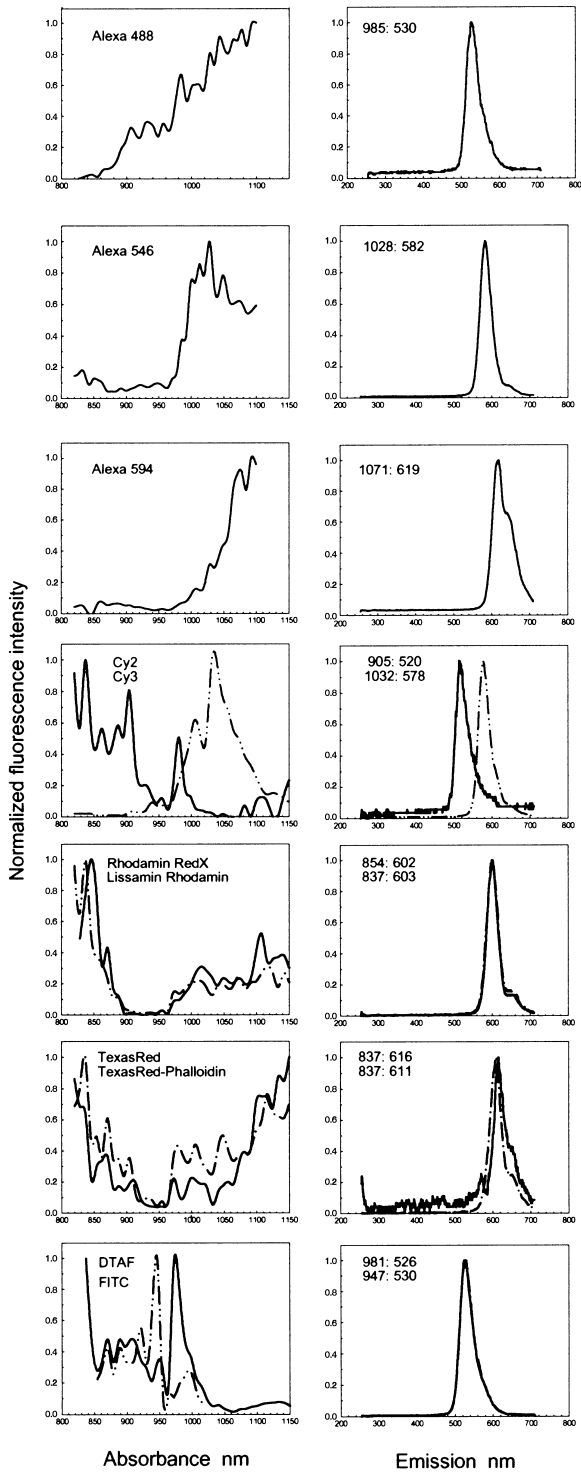


Fig. 4. TPE absorption and emission spectra of fluorochromes conjugated to an antibody (IgG). Explanations according to Fig. 3.

enhanced cyan fluorescent protein (ECFP), enhanced green fluorescent protein (EGFP) and MitoTracker Red. The efficiency of the 860 nm excitation with regard to the maximum of the respective fluorochrome was 26.7% for EGFP, 37.7%

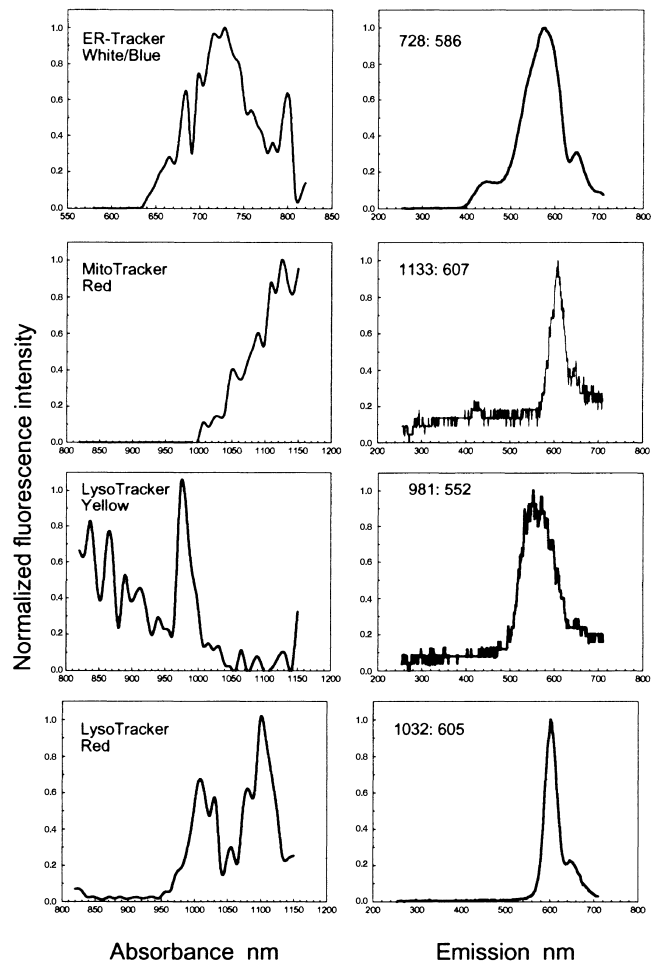


Fig. 5. TPE absorption and emission spectra of cell organelle tracker fluorochromes. Explanations according to Fig. 3.

for ECFP and < 1% for Hoechst 33342 and MitoTracker Red, according to the presented spectra and the GFPs (our own unpublished results).

In spite of low fluorescence yield, visualization of multiple labels is possible as demonstrated in Fig. 6. Cells of a clone permanently expressing the histone H2A tagged with enhanced cyan fluorescent protein (ECFP) (Bestvater *et al.*, 2002) were seeded onto a collagen gel matrix and supertransfected with a tubulin-enhanced green fluorescent protein (EGFP) chimera. The mitochondria were stained 12 h post-transfection with the live cell marker MitoTracker Red CMX and the cell nuclei with the DNA marker Hoechst 33342. The axial slicing steps could not be further reduced without having a significant impact on the stability of the fluorophores during the sequential collection of images in four channels. Each recorded image stack amounted to $512 \times 512 \times 64$ pixels (= 16 Mb); this equals 64 Mb for the complete set of images. According to the camera specifications and the slicing distance, the resulting dimensions of the smallest physical volume were

Table 2. TPE data table

Fluorochrome	TPE absorption maximum (nm)	Absorption shift TPE vs. 2 × OPE (nm)	TPE emission maximum (at excitation) (nm)	Emission shift TPE vs. OPE (nm)
Dyes				
Acridine Orange	837 > 882 >> 981	–	548 (837)	–
aminomethylcoumarin	703 < 722 >> 863	+4	458 (820)	+ 11
methylcoumarin				
Bodipy FL ^a	920 << 972	–38	526 (972)	+15
Bodipy TRoad	1032 << 1108	–70	684 (1032)	+61
DAPI	685 > 697	–31	467 (685)	+6
DCF2 (H ₂ DCFDA) ^a	1065	+65	532 (1065)	±0
Hoechst 33342	660 > 715	–40	497 (660)	+10
lissamine rhodamine	837 >> 1116	–24	600 (837)	+5
PhenGreen-FL	1074	+90	435 << 522 (1074)	+5
PhenGreen-FL + Fe	1074		440 (1074)	
propidium iodide	989 > 1015 >> 1099	–13	612 << 657 (981)	–5, + 40
quinacrine	678 (697)	–168	517 (837)	+14
rhodamine 123	913 (1090)	–101	536 (947)	+7
SNARF-1	< 837	–200	622 << 660 (837)	+10
Organelle trackers				
ER-Tracker white/blue	728	–20	586 (728)	+11
LysoTracker Yellow	972	–104	435 << 552 (981)	±0
LysoTracker Red	1010 < 1100	–	605 (1032)	+15
MitoTracker Red	1133	–22	444 (1065) << 608 (1133)	+9
Antibody-conjugated				
Alexa Fluor 488	985	+3	530 (985)	+15
Alexa Fluor 546	1028	–78	582 (1028)	+13
Alexa Fluor 594	1074	–114	619 (1074)	+9
Cy2-IgG	837 < 905 > 981	–73	520 (905)	+14
Cy3-IgG	1032	–84	578 (1032)	+5
F-DTAF-IgG	< 820; 820 > 837 > 972	–8	527 (981)	+7
FITC-IgG	947	–39	530 (947)	+5
RedX-IgG	845 >> 1108	–	602 (854)	±0
TexasRed-IgG	1108 (> 1150)	–	616 (837)	±0
TexasRed-Phalloidin	> 1150	–	611 (837)	+9

^aDissolved in DMSO.

0.213 μm × 0.213 μm × 0.500 μm (= 0.0227 μm³). A representative section taken at the same depth is shown for each channel as a raw data image (Fig. 6a–d). The signal-to-noise ratio in the various channels is very different. It must be taken into account that besides the absorption of energy, the local concentration of the respective dyes and their photo-physical parameters (quantum yield and extinction coefficient which determine fluorescence intensity) contribute to the image formation. Fluorescence intensity is highest for MitoTracker Red and lowest for Hoechst 33342. This might explain the apparent differences of these two images. In the case of the GFPs the situation is less striking; EGFP has about a threefold higher fluorescence intensity than ECFP, which obviously compensates the lower absorption. It must be stressed that the feasibility of the single-wavelength approach

is not yet a satisfactory solution for simultaneous imaging of multiply stained samples, as it is definitely suboptimal. Future efforts in laser development should ensure optimal excitation for each fluorophore.

The 3D representation of the optical slicing (Fig. 6e) gives a complex impression of the distribution of the four fluorochromes and their spatial relationship to each other. The fractal shape of the nucleus, with partial but not complete overlap of the labelled histone and the DNA, is noticeable. Dislocations among identical structures are caused by intracellular movements taking place in the living cells while they are recorded in the different channels. Faster scanning partially overcomes this disadvantage, but significantly increases the background noise. In spite of the thorough selection of parameters, a slight bleaching but no apparent photodamage was observed. The

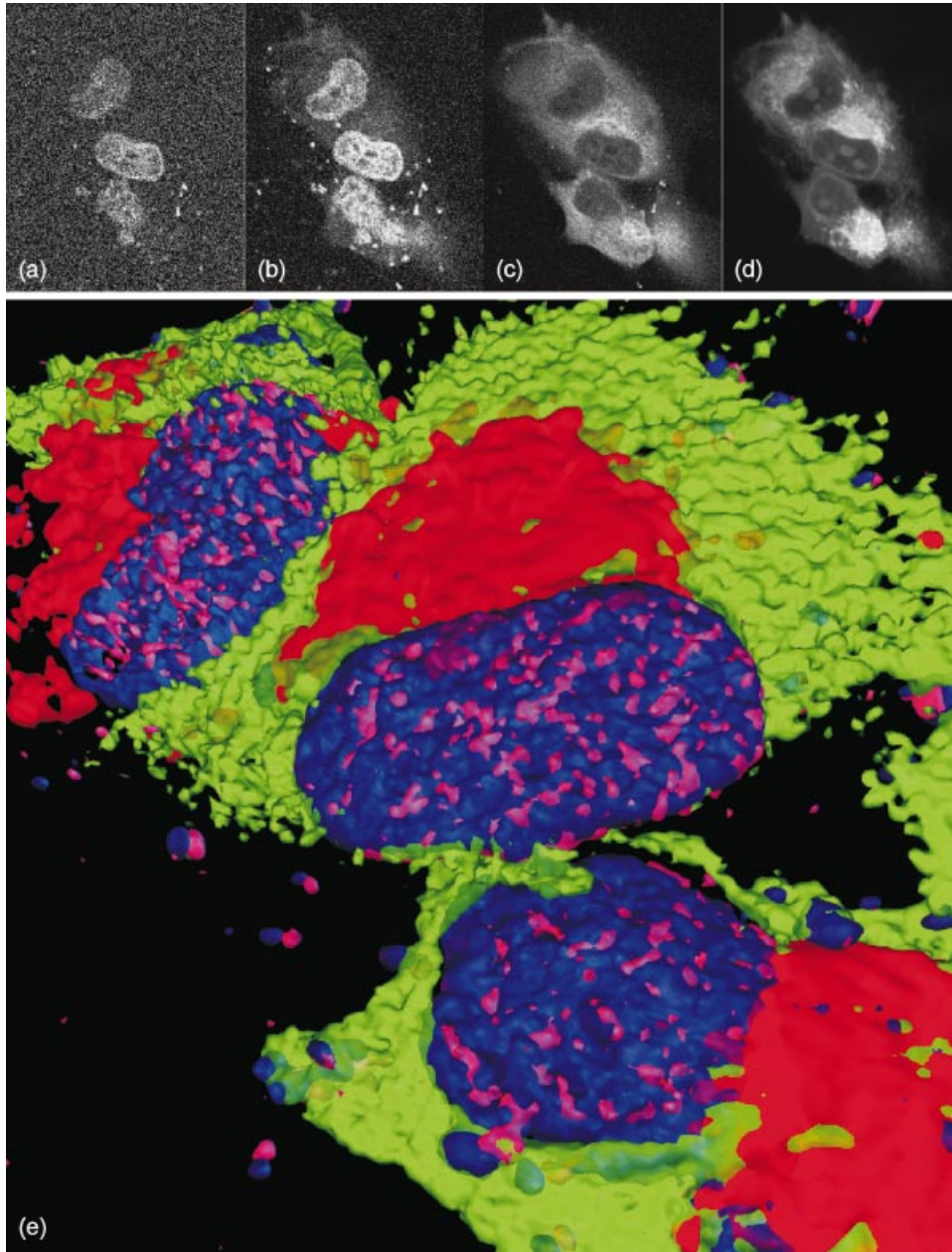


Fig. 6. Three-dimensional reconstruction of LCLC-103H cells in four different fluorescence channels. The cells permanently expressing the histone H2A tagged with ECFP were seeded onto a collagen gel matrix and supertransfected with tubulin–EGFP. Twelve hours post-transfection, the mitochondria were stained with the live cell marker MitoTracker Red CMX and the DNA by Hoechst 33342. A TPLSM equipped with a water-immersion objective (60×/NA 1.2) was used to record the raw data at an excitation wavelength of 860 nm. The fluorescence was monitored at different emission wavelengths with 5 mW incident laser power. The dimensions of the imaged volume were $108.6 \mu\text{m} \times 108.6 \mu\text{m} \times 31.5 \mu\text{m}$. (a) to (d) Representative raw data images are shown obtained at the same sample depth for (a) Hoechst 33342 emission (440/10 nm), (b) ECFP-emission (470/30 nm), (c) EGFP-emission (510/20 nm) and (d) MitoTracker Red emission (620/60 nm). (e) Volume reconstruction: the raw data were spatially reconstructed, the isosurfaces were rendered and a false colour LUT was applied to the different channels: (i) pink, DNA of cell nuclei stained with Hoechst 33342; (ii) blue, nuclear histones visualized by the chimeric construct H2A–ECFP; (iii) green, microtubuli visualized by tubulin–EGFP; (iv) red, mitochondria stained with MitoTracker Red.

limitations of the low excitation efficiency become obvious when the mitochondria and the microtubuli are viewed. Neither network could be resolved in detail, although the general distribution and the spatial relationship can be seen clearly. As

already discussed (Piston, 1999), in practice, the resolution obtained by TPE is inferior to conventional confocal microscopy. The biological advantages, however, lie in the reduced cell damage and the extended observation period for live cell microscopy.

Acknowledgements

We would like to thank Tobias A. Knoch (DKFZ) for providing the histone-ECFP construct. We are also grateful to Christina Barther, Agnes Carlisle (Newbury, U.K.) and Anna Heckel-Pompey (DKFZ) for critical reading the manuscript. The project received financial support from Silicon Graphics (SGI), Nikon and Newport to H.A., and from the Bundesministerium für Bildung und Forschung (BMBF) grants 13 N7447/5 to H.A. and 13 N7308/6 to T.F.

References

- Albota, M.A., Xu, C. & Webb, W.W. (1998) Two-photon fluorescence excitation cross sections of biomoolecular probes from 690 to 960 nm. *Appl. Opt.* **37**, 7352–7356.
- Bestvater, E., Knoch, T.A., Langowski, J. & Spiess, E. (2002) Construct conversions caused by simultaneous cotransfection: 'GFP-walking'. *Biotechniques*, **32**, 830–836.
- Birge, R.R. (1986) Two-photon spectroscopy of protein bound chromophores. *Acc. Chem. Res.* **19**, 138–146.
- Brown, E.B., Campell, R.B., Tsuzuki, Y., Xu, L., Carmeliet, P., Fukumura, D. & Jain, R. (2001) *In vivo* measurement of gene expression, angiogenesis and physiological function in tumours using multiphoton laser scanning microscopy. *Nature Med.* **7**, 864–868.
- Centonze, V.E. & White, J.G. (1998) Multiphoton excitation provides optical sections from deeper within scattering specimens than confocal imaging. *Biophys. J.* **75**, 2015–2024.
- Denk, W., Piston, D.W. & Webb, W.W. (1995) Two-photon molecular excitation in laser scanning microscopy. *Handbook of Biological Confocal Microscopy* (ed. by J. B. Pawley), pp. 445–458. Plenum Press, New York.
- Denk, W., Strickler, J.H. & Webb, W. (1990) Two-photon laser scanning fluorescence microscopy. *Science*, **248**, 73–76.
- Denk, W. & Svoboda, K. (1997) Photon upmanship. Why multiphoton imaging is more than a gimmick. *Neuron*, **18**, 351–357.
- Fisher, W.G., Wachter, E.A., Lytle, F.E., Armas, M. & Seaton, C. (1998) Source-corrected two-photon excited fluorescence measurements between 700 and 880 nm. *Appl. Spect.* **52**, 536–545.
- Gratton, E., Barry, N.P., Beretta, S. & Celli, A. (2001) Multiphoton fluorescence microscopy. *Methods*, **25**, 103–110.
- Hell, S.W., Booth, M., Wilms, S., Schmetter, C.M., Kirsch, A.K., Arndt-Jovin, D.J. & Jovin, T. (1998) Two-photon near and far-field fluorescence microscopy with continuous-wave excitation. *Opt. Lett.* **23**, 1238–1240.
- König, K. (2000) Multiphoton microscopy in life sciences. *J. Microsc.* **200**, 82–104.
- Malak, H., Castellano, F.N., Gryczynski, I. & Lakowicz, J.R. (1997) Two-photon excitation of ethidium bromide labeled DNA. *Biophys. Chem.* **67**, 35–41.
- Patterson, G.H. & Piston, D.W. (2000) Photobleaching in two-photon excitation microscopy. *Biophys. J.* **78**, 2159–2162.
- Periasamy, A., Skoglund, P., Noakes, C. & Keller, R. (1999) An evaluation of two-photon excitation versus confocal and digital deconvolution fluorescence microscopy imaging in *Xenopus* morphogenesis. *Microsc. Res. Techn.* **47**, 172–181.
- Piston, D.W. (1999) Imaging living cells and tissues by two-photon excitation microscopy. *Trends Cell Biol.* **9**, 66–69.
- Sheppard, C.J.R. (1977) The use of lenses with annular aperture in scanning optical microscopy. *Optik*, **48**, 329–334.
- Smith, W.L. (1986) Two-photon absorption in condensed media. *Handbook of Laser Science and Technology* (ed. by J. Weber), pp. 229–258. CRC, Boca Raton, Florida.
- Straub, M., Lodemann, P., Holroyd, P., Jahn, R. & Hell, S.W. (2000) Live cell imaging by multiphoton microscopy. *Eur. J. Cell Biol.* **79**, 726–734.
- Williams, R.M., Piston, D.W. & Webb, W.W. (1994) Two-photon molecular excitation provides intrinsic 3-dimensional resolution for laser-based microscopy and microphotochemistry. *FASEB J.* **8**, 804–813.
- Williams, R.M., Zipfel, W.R. & Watt, W.W. (2001) Multiphoton microscopy in biological research. *Curr. Opin. Chem. Biol.* **5**, 603–608.
- Xu, C. & Webb, W. (1996) Measurement of two-photon excitation cross sections of molecular fluorophores with data from 690 to 1050 nm. *J. Opt. Soc. Am. B.* **13**, 481–491.
- Xu, C., Zipfel, W., Shear, J.B., Williams, R.M. & Webb, W.W. (1996) Multiphoton fluorescence excitation: new spectral windows for biological non-linear microscopy. *Proc. Natl. Acad. Sci. USA*, **93**, 10763–10768.